Effect of Iron Pentacarbonyl on Soot Formation behind Shock Waves

G. L. Agafonov, V. N. Smirnov, and P. A. Vlasov

Semenov Institute of Chemical Physics, Russian Academy of Sciences, Kosygin str. 4, 119991 Moscow, Russia, E-mail: iz@chph.ras.ru

1 Introduction

The use of metal-containing additives in combustion applications has a long and at times controversial history. The influence of metal additives on soot formation in combustion has been studied for several practical and laboratory systems. Iron-bearing compounds turned out to be the most effective metal additives [1]. Although extensive studies have been performed, the mechanisms through which iron additives act in flames are not yet fully understood [2, 3]. Metal-containing compounds have long been used to suppress soot formation. Iron pentacarbonyl ($Fe(CO)_5$) has been widely used as a gaseous precursor for producing iron catalyst nanoparticles for the growth of carbon nanotubes in flames, in the HiPCO (high-pressure CO conversion) process, and in a plug-flow reactor. Recently, a few well-documented experimental studied of iron particle formation during the decomposition of $Fe(CO)_5$ behind shock waves were reported [4, 5].

Several kinetic schemes of the thermal decomposition of iron pentacarbonyl accompanied by nucleation and condensation were proposed [4, 6, 7]. Recently, a new detailed kinetic model of the thermal decomposition of iron pentacarbonyl and condensation of iron atoms appeared [8], which is free of the defects of the previous kinetic schemes. It is based on novel thermochemical data for iron pentacarbonyl $Fe(CO)_5$ and unsaturated iron carbonyls, including $Fe(CO)_n$, $n = 1$–4, $Fe_n(CO)_m$, $n = 1$–7, $m = 1$–5, and the iron clusters Fe_n, $n = 2$–7.

This kinetic scheme makes it possible to quantitatively describe all the available experimental data on the yield of iron atoms Fe and CO in the gas phase and the mean sizes of the iron nanoparticles formed in the course of iron atom condensation during the thermal decomposition of various mixtures of iron pentacarbonyl in argon behind incident and reflected shock waves at various temperatures and pressures.

This scheme is capable of accurately predicting the time histories of the concentration and mean size of iron particles in the mixture.

The aim of the present work was to examine the predictive possibilities of the new kinetic scheme of the thermal decomposition of iron pentacarbonyl with the formation of free iron atoms and then nanoparticles in the gas phase and to perform an experimental and computational study of the influence of iron pentacarbonyl additives on soot formation during propane pyrolysis behind reflected shock waves.

Correspondence to: P.A. Vlasov, iz@chph.ras.ru

2 Experimental

The details of experimental installation are described in [9]. The emission and absorption signals from the ensembles of soot and iron particles (λ = 632.8 nm) were recorded at the same cross section located at a distance of 15 mm from the endplate of the shock tube. From these measurements, the time dependences of the particle temperature (and, consequently, the gas temperature) and soot and iron particle yields were obtained.

The parameters of the gas behind the reflected shock wave were calculated from the incident shock velocity, with the composition of the test mixture being determined based on the ideal-flow shock-tube theory. The incident wave velocity was measured with a set of three piezoelectric gauges spaced 528 and 281 mm apart, with the last one being located 40 mm from the observation section. The distance from the endplate to the observation section was 15 mm. To determine the soot yield and the temperature of the soot particles, we used the double-beam absorption-emission technique.
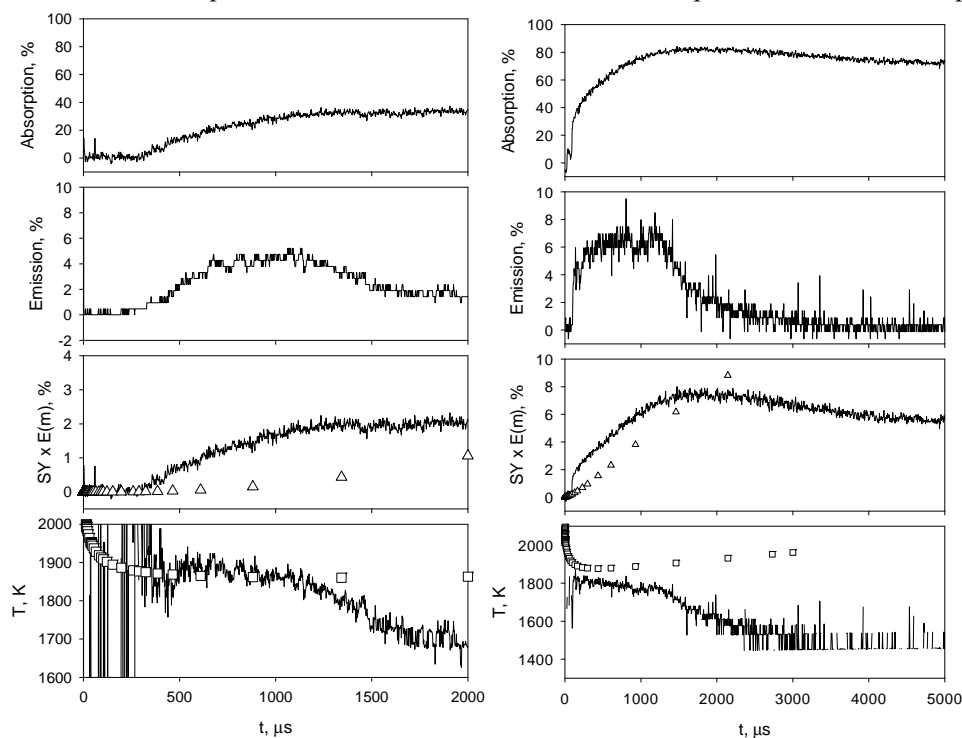
Fig. 1. Typical absorption and emission signals and the time dependences of the soot yield and temperature obtained from them for 1.66% C_3H_8 + 98.34% Ar (left) and 1.66% C_3H_8 + 0.3% $Fe(CO)_5$ + 98.04 %Ar (right) mixtures; initial temperatures are T_{50} = 2271 K and 2255 K, respectively; the total concentrations were $[M]_{50}$ = 2.76×10^{-5} and 3.17×10^{-5} mol/cm^3, respectively; wavelength, λ = 632.8 nm.

Figure 1 shows typical absorption (frame 1) and emission (frame 2) signals. The emission signal intensity is given in relative units, in percent with respect to the signal intensity from the calibration band lamp. The time histories of the soot yield and soot temperature were calculated under the standard assumptions: the soot particles are spherical and their optical properties are described in the Rayleigh law. Triangles in frame 3 and squares in frame 4 represent the calculated soot yield and gas temperature, respectively.

The observed decay in the emission signal is associated with the arrival of the rarefaction wave at an instant of time of ~1200 µs; as a result, the measured temperature decreases by about 100 K within the remaining ~800 µs; this, however, produces a minor effect on the absorption profile, since the test mixture density changes only slightly.

Since there is a considerable scatter in the available values of $E(m)$, we plotted the quantity $SY \times E(m)$ as a function of the time. Studying the formation of soot during the pyrolysis of toluene behind reflected shock waves, we estimated $E(m)$ as 0.37, in close agreement with the most recent data [9, 10]. This quantity has the advantage that it was determined under conditions similar to those used in the present experiments.

3 Kinetic model

The kinetic modeling was carried using a reaction scheme of soot formation developed in [10], supplemented by the reaction scheme of iron pentacarbonyl thermal decomposition accompanied by the formation of free iron atoms and the formation and decomposition of iron nanoparticles formed from free iron atoms and from iron pentacarbonyl decomposition fragments [8].

Our kinetic model postulates that the soot precursors are PAHs formed by reactions between small saturated PAHs and PAH radicals or between PAH radicals only. The reactions of formation of soot precursors are assumed to be irreversible. The reactions of surface growth can take place at active sites formed in reactions with hydrogen atoms. Thus, two different ensembles of soot precursors are considered in the model: soot precursors with and without active sites. Soot particles have a developed surface and each site on their surface can be activated and deactivated in the reactions with gas-phase species. At present, it is difficult to define an exact boundary between soot precursors and soot particles, but in the future, such a separation, at least formal, into several ensembles of particles may prove useful for improving the kinetic model.

The kinetic model of soot formation is based on a gas-phase reaction mechanism that describes the pyrolysis and oxidation of initial hydrocarbons, in particular propane, and the formation and growth of PAHs through different reaction pathways up to coronene. The formation, growth, oxidation, and coagulation of soot precursors and soot particles were described using the discrete Galerkin technique [9, 10].

The core of the gas-phase reaction mechanism is the reaction sequence of PAH formation in laminar premixed acetylene and ethylene flames (HACA). At the same time, the mechanism was extended to include a number of additional channels of PAH formation and growth (up to coronene) and a comprehensive set of reactions involving C_3-, C_5-, and C_7-hydrocarbons. More specifically, the mechanism included (1) the alternating H-abstraction/C_2H_2-addition (HACA) route, resulting in the successive growth of PAHs; (2) the combination reactions of phenyl with C_6H_6; (3) the cyclopentadienyl recombination; and (4) the ring-closure reactions of aliphatic hydrocarbons. The principles underlying this mechanism are outlined in [10].

The modified gas-phase reaction mechanism was comprised of 3320 direct and reverse reactions between 274 different species, with the rate coefficients of some important reactions being pressure-dependent.

Soot precursors are formed by radical−molecule reactions of different PAHs, starting from phenylacetylene, acenapthalene, and ethynylnapthalene, up to coronene and by radical−radical reactions (from cyclopentaphenanthrene up to coronene radicals). These reactions result in the formation of polyaromatic molecules containing from 16 to 48 carbon atoms, which are stabilized by the formation of the new chemical bonds. Iron nanoparticles are also considered as soot precursors. Soot precursors are activated in reactions with H and OH radicals and deactivated in reactions with H, H_2 and H_2O. Soot precursors grow via reactions with C_2H_2, C_4H_2, and C_6H_2 (the concentrations of which are rather high in the pyrolysis and oxidation of aliphatic and aromatic hydrocarbons), reactions with polyaromatic molecules and radicals, and the process of coagulation. Soot precursors are oxidized by O and OH radicals. They are transformed into soot particles through internal conversion reactions, in which the number of active sites in the reacting system is preserved. Soot particles grow in the reactions with C_2H_2, C_4H_2, C_6H_2 and PAH molecules and radicals. All types of soot particles were postulated to participate in coagulation.

4 Results and discussion

The kinetic modeling showed that the novel kinetic scheme of iron pentacarbonyl thermal decomposition with the formation of free iron atoms [8] and their subsequent condensation into iron nanoparticles quantitatively describes the available experimental data [4, 5]. A comparison of the experimentally measured [4, 5] and calculated concentrations of Fe atoms and CO for two different $Fe(CO)_5$/Ar mixtures at various temperatures and pressures behind incident shock wave and mean iron particle diameter for two different translation energy accommodation coefficients is illustrated in Figs. 2 and 3, respectively.
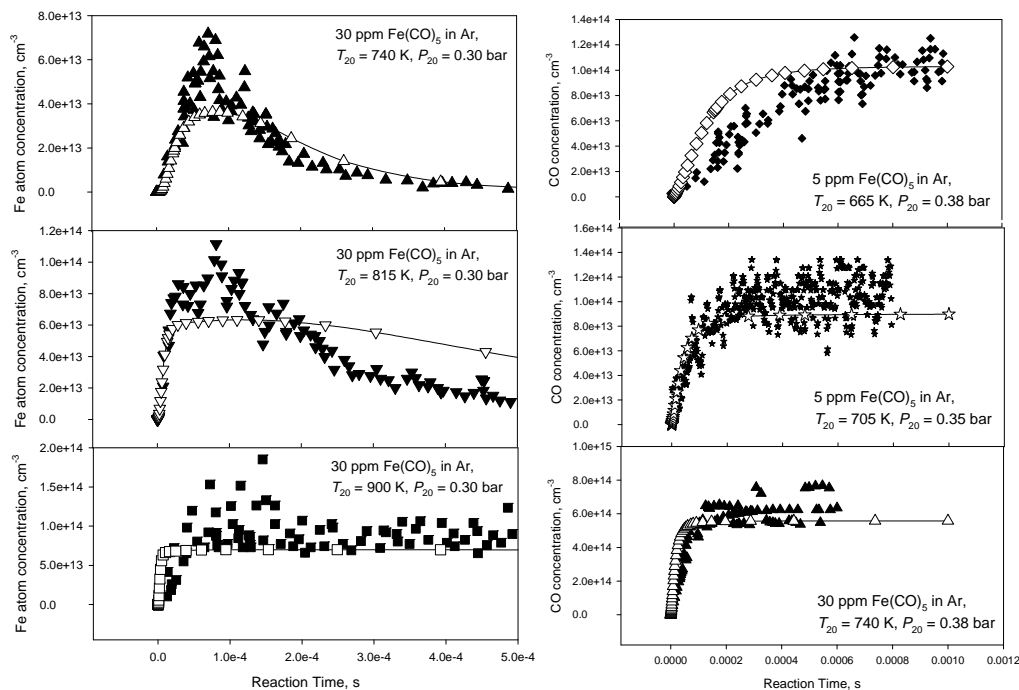
Fig. 2. Comparison of experimentally measured [4] (closed symbols) and calculated (present work, open symbols and lines) concentrations of Fe atoms and CO for two different $Fe(CO)_5$/Ar mixtures at various temperatures and pressures behind the incident shock wave.
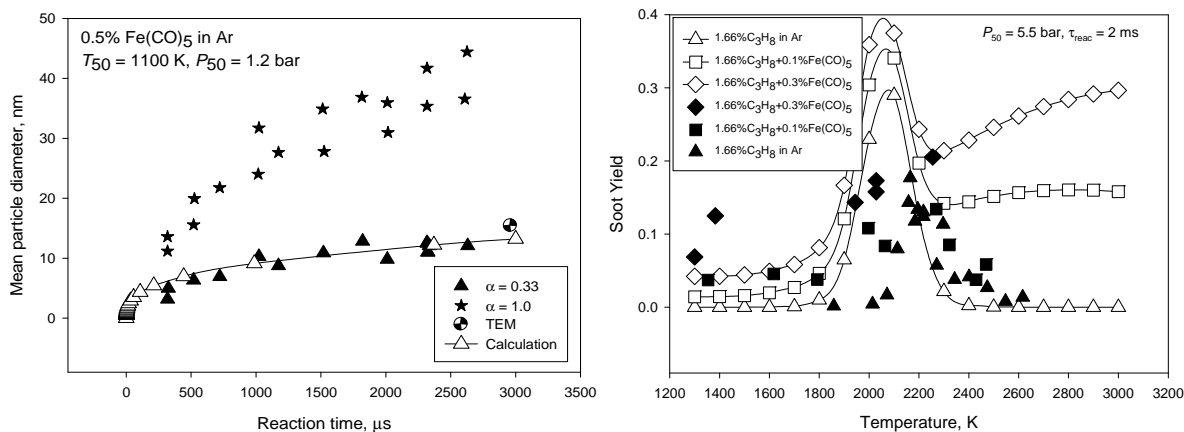
Fig. 3 (left). Comparison of the experimentally measured (closed symbols) mean iron particle diameter for two different translational energy accommodation coefficients with the results of TEM determination and with the results of our kinetic modeling (open symbols).

Fig. 4 (right). Comparison of the experimentally measured (closed symbols) and calculated (open symbols) soot yields for the pyrolysis of a 1.66%C_3H_8/Ar mixture without and with 0.1%$Fe(CO)_5$ and 0.3%$Fe(CO)_5$ additives at different temperatures the behind reflected shock wave.

A well-pronounced promoting effect of the small iron pentacarbonyl additives on soot formation during the pyrolysis of propane/Ar mixtures was observed, especially at low and high temperatures, at which soot is practically not formed in the absence of iron pentacarbonyl (Fig. 4).

The experiments on soot formation during pyrolysis of propane/Ar mixtures with the additives of oxygen O_2, toluene C_7H_8, and iron pentacarbonyl $Fe(CO)_5$ demonstrated a strong inhibiting effect of oxygen additives (Fig. 5b) and a well-expressed promoting effect of iron pentacarbonyl (Fig. 5c) and toluene additives on soot formation (Fig. 5d). In the case of iron pentacarbonyl additives (Fig. 5c), the induction period of soot formation is practically absent. This implies that, immediately after the formation of iron nanoparticles, the process of condensation of carbon-containing species from the gas phase on the surface of these iron particles begins. Iron particles are coated and gradually transformed into soot nuclei and young soot particles.
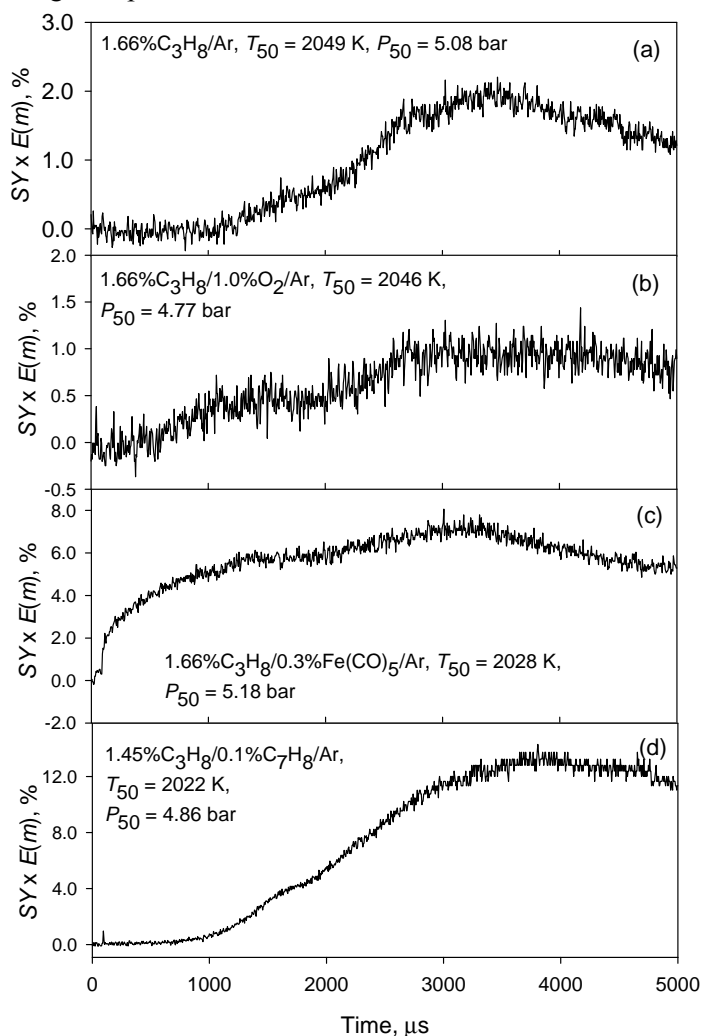
Fig. 5. Experimental time dependences of the soot yield during pyrolysis of propane/Ar mixtures with different additives.

To explain the promoting effect of iron pentacarbonyl additives on soot formation during the pyrolysis of propane/Ar mixtures behind shock waves, we assumed that the nascent iron nanoparticles serve as nuclei for the formation of soot particles. This assumption is confirmed by the experimental results reported by Roth and coworkers [5], who performed TEM analysis of iron−carbon particles and found that such particles consists of an iron core coated with a carbon layer. Our model qualitatively correctly describes the experimentally observed promoting effects of iron pentacarbonyl additives on

soot formation during propane pyrolysis behind reflected shock waves (Fig. 4). The effects of small iron clusters on the chemical composition of the reactive mixture [11, 12] may turn out to be also important. However, the role of such processes should be studied separately, when more information will be available.

5 Conclusions

A strong influence of iron pentacarbonyl additives on soot formation during the pyrolysis of propane/Ar mixtures behind shock waves was revealed. A novel kinetic mechanism of the thermal decomposition of $Fe(CO)_5$ and the formation of free iron atoms and iron nanoparticles was tested. This mechanism correctly describes the available experimental data. A qualitative explanation of the experimentally observed effects of $Fe(CO)_5$ additives on soot formation was proposed. In our opinion, the nascent iron nanoparticles serve as soot precursors for further surface growth with the formation of soot particles. The influence of small $Fe_n(CO)_m$ fragments and small Fe_n clusters on soot formation process is less probable because of a rather short life time of these species.

Acknowledgments

References

[1] Tanke D, Wagner HGg, Zaslonko IS. (1998). Mechanism of the action of iron-bearing additives on soot formation behind shock waves. Proc. Combust. Inst. 27: 1597.

[2] Kim KB, Masiello KA, Hahn DW. (2008). Reduction of soot emissions by iron pentacarbonyl in isooctane diffusion flames. Combustion and Flame. 154: 164.

[3] Linteris GT, Rumminger MD, Babushok VI. (2008). Catalytic inhibition of laminar flames by transition metal compounds. Progress in Energy and Combustion Science. 34: 288.

[4] Giesen A, Herzler J, Roth P. (2003). Kinetics of the Fe-atom condensation based on Fe-concentration measurements. J. Phys. Chem. A. 107: 5202.

[5] Starke R, Kock B, Roth P. (2003). Nano-particle sizing by laser-induced-incandescence (LII) in a shock wave reactor. Shock Waves. 12: 351.

[6] Krestinin AV, Smirnov VN, Zaslonko IS, (1991). A kinetic model of $Fe(CO)_5$ thermal decomposition and iron particle formation in shock tubes. Sov. J. Chem. Phys., 8: 689.

[7] Rumminger MD, Reinelt D, Babushok V, Linteris GT, (1999). Numerical study of the inhibition of premixed and diffusion flames by iron pentacarbonyl. Comb. Flame., 116: 207.

[8] Wen JZ, Goldsmith CF, Ashcraft RW, Green WH. (2007). Detailed kinetic modeling of iron nanoparticle synthesis from the decomposition of $Fe(CO)_5$. J. Phys. Chem. C. 111: 5677.

[9] Agafonov GL, Smirnov VN, Vlasov PA. (2010). Shock tube and modeling study of soot formation during pyrolysis of propane, propane/toluene and rich propane/oxygen mixtures. Combustion Science and Technology. 182: 1645.

[10] Agafonov GL, Smirnov VN, Vlasov PA. (2011). Shock tube and modeling study of soot formation during the pyrolysis and oxidation of a number of aliphatic and aromatic hydrocarbons. Proc. Combust. Inst. 33: 625.

[11] Chretien S, Salahub DR. (2003). Kohn–Sham density-functional study of the adsorption of acetylene and vinylidene on iron clusters, Fe_n/Fe_n^+ (n = 1–4). J. Chem. Phys., 119: 12279.

[12] Chretien S, Salahub DR. (2003). Kohn–Sham density-functional study of the formation of benzene from acetylene on iron clusters, Fe_n/Fe_n^+ (n = 1–4). J. Chem. Phys., 119: 12291.